

Review**Controlling Laser Filamentation Induced Strong THz Fields**M. Massaouti¹ and S. Tzortzakis^{1, 2, *}

¹*Institute of Electronic Structure and Laser (IESL),
Foundation for Research and Technology – Hellas (FORTH),
P.O. Box 1527, 71110 Heraklion, Greece*

²*Department of Materials Science and Technology,
University of Crete, 71003 Heraklion, Greece*

(Received September 17, 2013)

This article reviews recent advances on tuning intense THz pulses generated from 2-color femtosecond laser filaments in gases. In particular, extended tunability of the THz pulses is shown via filamentation molding and the use of cleverly engineered metamaterials and eutectics.

DOI: 10.6122/CJP.52.490

PACS numbers: 52.38.Hb, 42.65.-k, 81.05.Xj, 78.67.Pt

I. INTRODUCTION

During the past decade, thanks to the tremendous technological development in photonics and materials science, terahertz (THz) radiation became routinely accessible, opening new frontiers in several research fields, including chemistry [1], biology [2], medicine [3] and materials science [4]. The continuously increasing interest for terahertz waves and their applications is fostered by their non-invasive nature (1 THz=4.43 meV photon energy) and their ability to penetrate through many materials [5], which are usually opaque in the infrared and visible. Additionally, several physical and chemical processes, not accessible before, are closely related to the low frequency dynamic modes such as crystalline lattice or inter-molecular vibrational modes, hydrogen bonding stretches, large-scale motions of an entire macromolecule, which are lying in this low-frequency range.

Up to date, numerous techniques have been tested and developed as THz sources and many of them, such as photoconductive antennas and optical rectification, are widely employed in various laboratories around the world. Using techniques like electro-optic (e.o.) [6] or photoconductive sampling [7], it is possible to coherently detect in the time domain the generated THz pulses, giving a direct access to the amplitude and more importantly the phase of the electric field. Yet, there is still a stumbling block for many applications in the THz regime due to the relatively low THz peak power that most of the existing techniques exhibit, with energies per pulse barely reaching the nano-Joule regime, while their further development is hindered by the lack of natural occurring materials exhibiting strong electric or magnetic response in the THz range.

*Electronic address: stzortz@iesl.forth.gr

In the past years, various table-top approaches have been followed in order to successfully scale up the strength of the THz pulse energy [8] with one of the most promising ones being the 2-color femtosecond filament plasma based THz source. This source is based on the use of amplified lasers where THz emission originates from the transverse plasma current which is formed by an asymmetric 2-color electric field filament. The 2-color filament induced plasma THz emission yields super-broadband spectra, reaching up to 200 THz [9], while extremely low-frequencies (< 0.1 THz) are produced [10]. Basically, this source produces a broadband electromagnetic THz radiation with electric field intensities up to 1 MV/cm [11], making it attractive for a wide range of experiments.

The aim of this review paper is to introduce the versatility of the 2-color femtosecond filament plasma based THz source through the tailoring of the plasma string which naturally governs the macroscopic properties of the emitted THz pulse. In addition, taking advantage of the broadband feature of the source and its ability to be combined with other synchronized optical pulses (covering a large spectral range of the E/M spectrum), we will present the ability to control the emitted THz wave through the use of artificially fabricated materials like THz metamaterials [12] and eutectics.

II. EXPERIMENTAL SYSTEM

In Figure 1 is shown the terahertz time-domain spectroscopic (THz-TDS) system developed in our group, which is based on a pump-probe coherent detection approach where intense, s-polarized THz pulses are generated through 2-color gas filaments. The setup uses a powerful amplified kHz Ti:Sa laser system delivering 35 fs pulses at 800 nm central wavelength and energy of 2.3 mJ per pulse. The initial beam is split in two arms (10% and 90% respectively). The most intense one, with energy equal to 1.3 mJ and a Gaussian beam profile with a diameter of 6.6 mm, is focused in ambient air with a positive lens of 200 mm focal length and partially doubled in frequency in a BBO crystal (50 μ m thick) to produce a 2-color filament and subsequently, THz radiation. The optimum ratio between the fundamental and the second harmonic amplitudes is 9 to 1. The second arm, after being further attenuated is used for probing the THz-induced birefringence in an electro-optic (e.o.) crystal and monitoring the time profile of the THz electric field [13]. For the collection, collimation and refocusing the generated THz beam in the e.o. detection crystal, a set of four parabolic mirrors is used, as depicted in Figure 1. The whole setup is enclosed in a purged gas (e.g. N₂) chamber for eliminating THz absorption from water vapor [14].

Using this THz setup, the electric field emitted from the 2-color filament is estimated to be up to 200 kV/cm for an input laser pulse energy of 1.3 mJ/pulse. In Figure 2 are presented two examples where the same emitted signal has been recorded with a thick ZnTe crystal (500 μ m) and a thin GaP crystal (100 μ m). The measured electric field inherently depends on the crystal thickness (phase matching between the two pulses) and the presence of optical phonon modes. Thus, although with a thin GaP crystal we are able to detect higher frequencies (up to 8 THz) compared to ZnTe (see Figure 2(b)) -which has optical

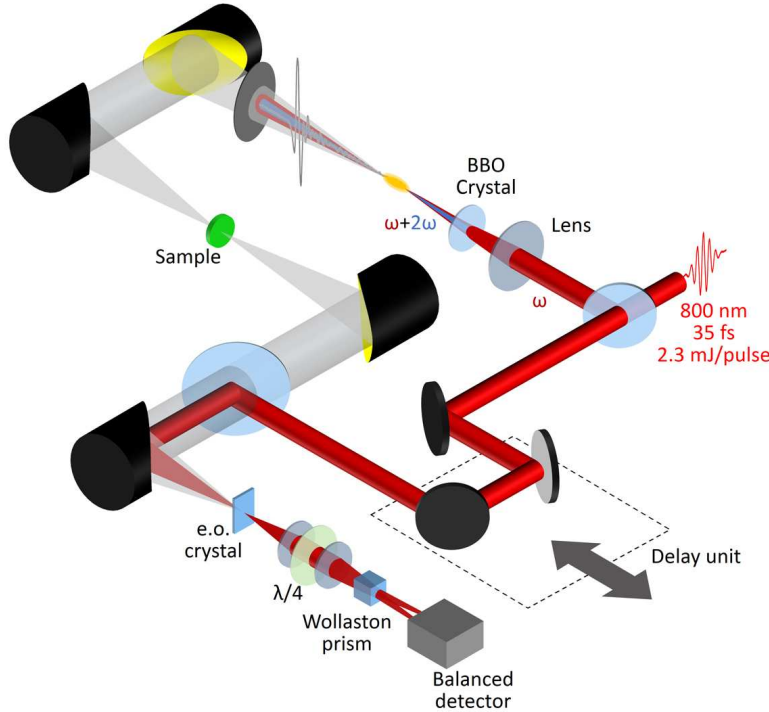


FIG. 1: Schematic representation of the THz-TDS experimental set-up.

phonon modes at lower frequencies- a signal with higher signal to noise ratio is recorded in the case of the ZnTe crystal (see Figure 2(a)) due to its thickness and its higher electro-optic coefficient compared to the GaP crystal. By applying a Fourier transform to these electric fields, one obtains the spectral distribution of the THz pulse (Figure 2(b)) and as one can see, the detected THz pulse duration clearly depends on the properties of the e.o. crystal used. We should note here that other techniques allowing a much broader band detection [15], have revealed frequency components up to 30 THz, using similar sources.

An estimation of the THz peak electric field can be directly deduced from the time domain trace, the measured energy and the estimation of the focused beam diameter. Using a commercially available THz-sensitive pyroelectric detector (Gentec-EO, SPI-A-62THz), we have measured the THz pulse energy to be 80 nJ for an input laser pulse energy of 1.3 mJ. In order to measure the diameter of our focused THz beam, a knife edge technique is used where a razor blade is scanning across the focused THz beam and the respective THz power is measured by the aid of the pyroelectric detector. For a Gaussian-like beam profile, the extracted full width half maximum (FWHM) is equal to 205 μm and at $1/e^2$ 435 μm . This size corresponds to a diffraction limited spot for a THz beam at 1.7 THz, which is in good agreement with the THz spectra presented above. Using the time trace measured with the thin GaP crystal (Figure 2(b)) and the full bandwidth measurement of the energy, the THz electric field is estimated to be equal to 200 kV/cm. One can scale up the energy

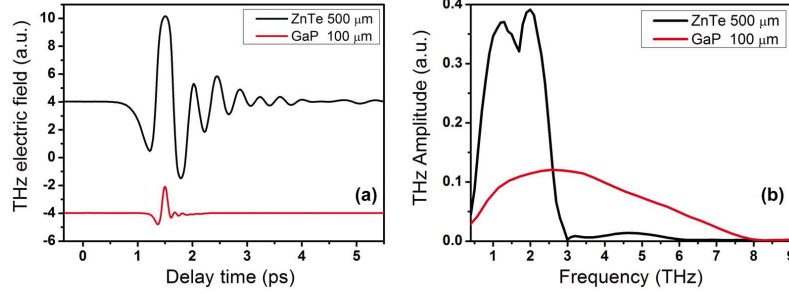


FIG. 2: (a) Recorded THz electric fields emitted from a 2-color filament and measured with two different electro-optic crystals, ZnTe and GaP. (b) Corresponding spectra from the Fourier transform of the electric fields.

content of the THz pulses using much higher input laser pulse energies (10 mJ) obtaining thus THz energies in excess of 1 μ J per pulse [11], hence opening the door to nonlinear THz optics and intriguing applications of high-field single-cycle THz pulses [16, 17].

III. TUNING THZ WAVES

III-1. Filamentation tailoring

The advantage of this source is not solely based on its intensity and broadband nature but also on using filaments which compared to the solid-state THz sources can be tailored, offering thus the possibility to tune the emitted THz pulses.

Microscopically, the generation of THz emission from a 2-color filament is the result of a transversal photocurrent. In a simplified view, one can describe the process like this: after the electrons get liberated at a certain velocity via the ionization process, they experience a drift from the remaining part of the laser electric field, which leads to a separation of charge in the transverse plane and the creation of a photocurrent [18]. The phase of the second harmonic field allows the projection of the photocurrent in any direction within the transverse plane. A direct consequence is that the technique offers a control on the polarization of the emitted THz pulse via the phase between the fundamental and its second harmonic [19–21].

Motivated by this microscopical picture, one could expect to achieve THz polarization control for short filament lengths via the accurate adjustment of the surrounding gas pressure. By changing the pressure, a wavelength dependent change of the refractive index is induced, which in turn will affect the phase of the synthesized laser field and consequently offer coherent control on the emitted THz pulse polarization. As shown in Figure 3, for relatively short plasma strings where the phase walk-off occurring in the plasma channel can be neglected, a $\pi/2$ polarization rotation of the emitted THz pulse is achieved over 650 mbar of the gas medium pressure with quasi constant THz power and linear pulse polarization. As demonstrated in [20], one can accurately predict the change in the polarization

angle of the emitted THz pulses by just calculating the dispersion between the ω and 2ω laser fields using the pressure dependent Sellmeier equation.

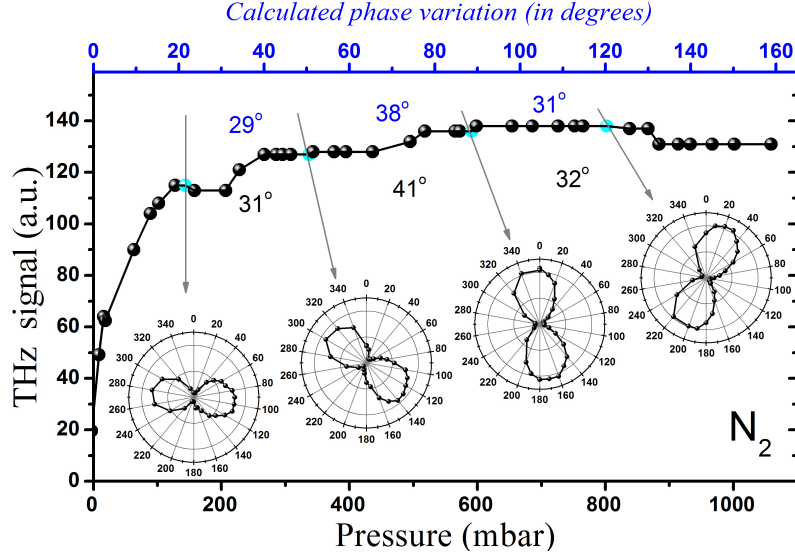


FIG. 3: Detected THz power as function of nitrogen gas pressure (dots-line) and THz pulse polarization states at different pressure levels of N_2 . The upper axis (blue on-line) represents the calculated phase variation.

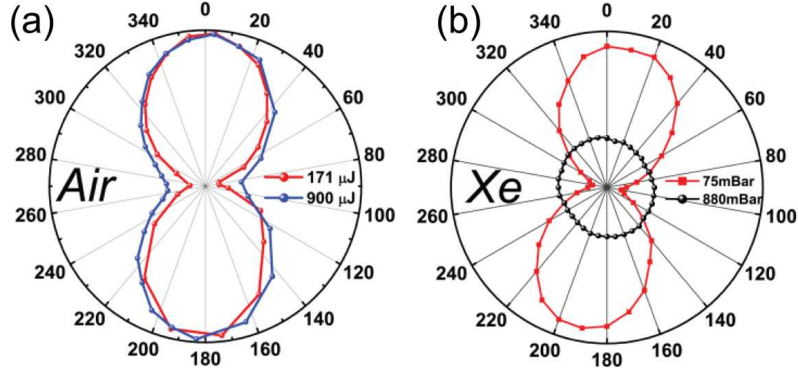


FIG. 4: (a) Normalized values of THz beam polarization state as measured for two different levels of input laser pulse energy in air, at atmospheric pressure. (b) The linear polarization (red curve) state of the THz beam pulse at low pressure in comparison to the circular polarized THz beam pulse (black curve) as recorded at 880 mbar in Xenon.

Nevertheless, at higher input laser pulse energies where the filament length is inherently longer, a degenerative behavior can be observed associated to the phase mismatch

within the elongated source. This is also accompanied with the appearance of ellipticity in the polarization of the beam, as one can see in Figure 4(a), where THz normalized polarization diagrams are presented for two different levels of laser pulse input energy at atmospheric pressure air. The observed ellipticity simply arises from the birefringence of the filament itself [22]. Furthermore, it is known from the literature that the saturation intensities within the filament are much lower for gases with low ionization potential (e.g. Xenon (12.13 eV)) and the excess of input laser energy leads to an extension of the plasma length as was shown by numerical simulations [23]. Consequently, using a gas such as Xenon, we have been able to clearly extend the plasma length and thus increase the accumulated birefringence and obtain fully circularly polarized THz beams, as presented in Figure 4(b). This result is of main importance since circularly polarized THz light can be used for instance to study circular dichroism in various molecular and biological systems.

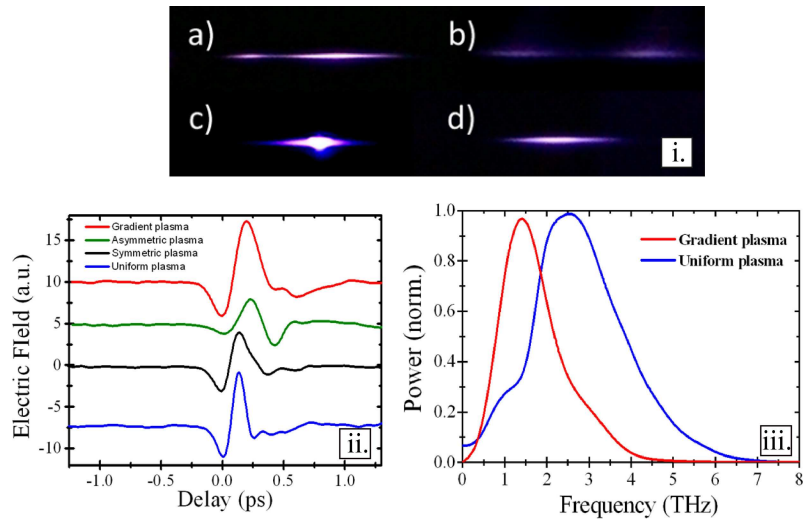


FIG. 5: (i) Fluorescence images of filament plasma string distributions,(a) asymmetric (b) symmetric double peaks, (c) uniform and (d) gradient, obtained under various experimental conditions and (ii) their respective electric field traces. In (iii) are shown the corresponding spectra of the uniform and gradient plasma recorded electric fields.

As we have seen, except the microscopical picture of THz generation through 2-color gas filaments, equally important is the macroscopic filament-THz propagation effect, which practically affects not only the polarization of the emitted THz pulses but also their bandwidth [24] and energy scale [10, 25]. In order to investigate how the THz field is modified for different plasma string distributions, we have followed the approach of filamentation tailoring. In most experimental situations, the highly dynamical nature of the filamentation process leads to a non-uniform plasma distribution with strong gradients along the propagation path. Furthermore, due to the high intensities reached within a filament, it is impossible to insert optics in order to gain control on the filamentation process. Consequently, one needs to find external means to obtain control on this process. For example,

the introduction of distortion in the laser beam wavefront can lead to the control of the electron density distribution, which in turn yields different THz waveforms [24]. The waveform recorded for diverse electron density distributions are presented in Figure 5(ii) along with a CCD picture of the respective plasma strings (Figure 5(i)). Hence various THz waveforms are produced offering wide tunability in terms of the spectral distribution. As observed in Figure 5(iii), the uniform plasma distribution offers a wider bandwidth and a different central frequency compared to the gradient case.

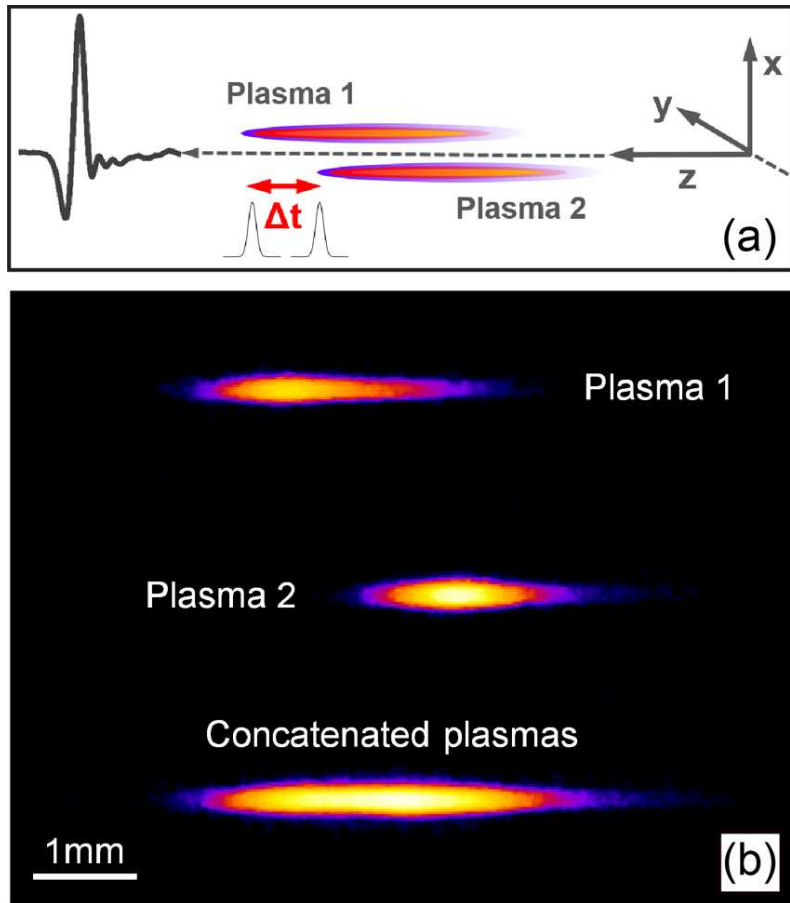


FIG. 6: (a) Schematic representation of the spatial and temporal arrangement of two independent plasma strings and (b) their respective fluorescence images along with the concatenated one as recorded with a CCD camera.

Following the same idea of plasma string tailoring we studied the effect of the extension of the length of the plasma string on the THz emission. In order to keep a uniform electron density distribution we used the approach of coherently linking two similar uniform filaments along the propagation axis (z axis on Figure 6(a)). This concatenation effect, which requires appropriate spatiotemporal adjustment of the 2 single filaments, results in the enhancement by one order of magnitude of the yielded THz pulse power and consider-

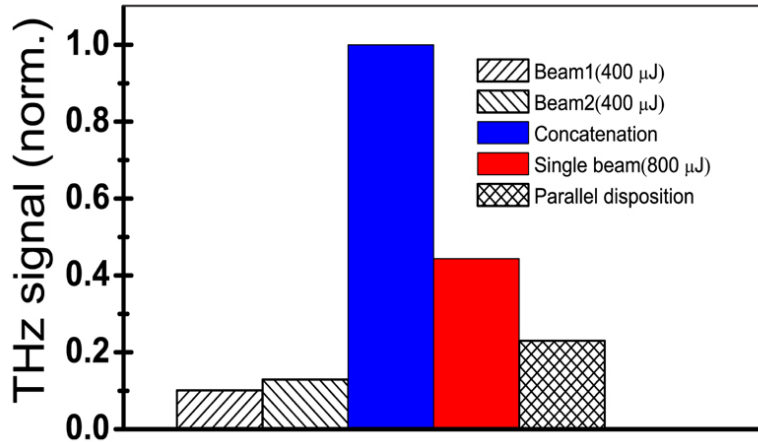


FIG. 7: Recorded THz signal for different spatial distributions of the two plasma strings and for each plasma string individually.

ably more than the strength of a single filament having an input laser energy equivalent to the sum of the two filaments (see Figure 7).

III-2. THz metamaterials

Another approach to control terahertz radiation is by using metamaterials which are specifically tailored for the THz regime [26]. Metamaterials are artificially fabricated materials composed of subwavelength structures, periodically arranged, exhibiting unique electromagnetic properties that cannot be found in nature. Up to date, a large variety of metamaterials have been designed and applied as manipulating devices of THz waves, including phase modulators [27], polarizers [4], absorbers [28, 29], and active frequency THz devices which can be controlled by light [30, 31].

Here we review two different schemes that allow the dynamic control of phase modulation [32] and resonance shifting [31] in the THz regime. Additionally, a self-organization approach for fabricating metamaterials will be presented, showing the potential of realizing simple subwavelength THz waveguides [33].

The first metamaterial is a classical metamaterial sample consisting of an array of split-ring-resonators (SRRs), fabricated from copper which are periodically arranged on top of a high resistivity GaAs substrate ($670 \mu\text{m}$). A sketch of the experimental approach, together with the exact dimensions of the SRR unit shell, is given in Figure 8. The metamaterial is designed so as to exhibit electric resonance response in the THz regime which can be dynamically tuned as photocarriers are injected within the GaAs substrate. The dynamic response of the metamaterial has been studied by placing the sample at the THz focus, at normal incidence and performing THz transmission measurements through the metamaterial sample as it is illuminated by an optical-pump laser beam (of central wavelength 800 nm) launched at 45° on the sample. The temporal synchronization of the THz

and the optical pump beams have been experimentally defined.

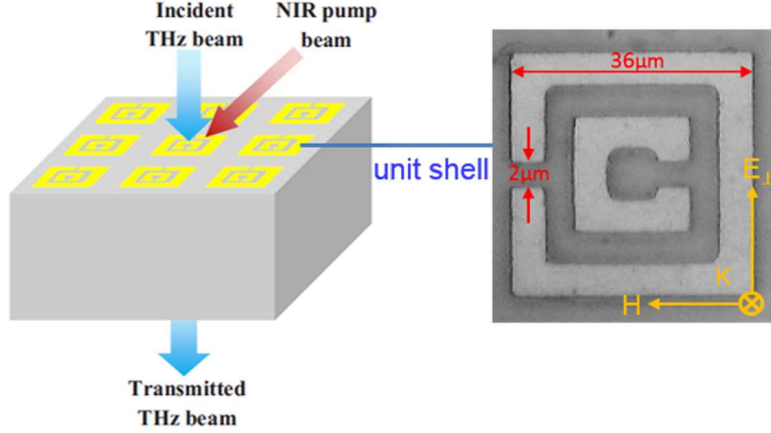


FIG. 8: Graphic representation of the metamaterial sample and the experimental geometry of the laser and THz beams.

In Figure 9(a) are shown the recorded THz amplitudes for different levels of excitation fluence. In the absence of photocarriers, the non-excited sample exhibits a broad resonance which is a dipole-like resonance of the structure, related to the finite length of the metallic element along the electric field direction. By injecting photocarriers, an amplitude modulation of the resonance is observed. By performing theoretical calculations (Figure 9(c)), using a simple Drude model, the experimental observations are explained as a result of the change of conductivity of the GaAs substrate, where increasing amounts of charges finally screen the existing resonance. More interestingly, a frequency shift is observed towards higher values (up to 50 GHz) as photocarriers are injected within the substrate (see Figure 9(b), (d)). As electrons and holes are created under photo-excitation within the substrate (over one penetration depth; 1 μm at 800 nm), beyond the changes in the conductivity, the complex index of refraction is expected to change as well, contributing to the observed phase shift. More details on these experiments and corresponding numerical simulations can be found in Ref. [32].

The second case we will discuss here involves a specifically designed metamaterial for which t-gap metallic SRRs are deposited on a dielectric substrate (sapphire). In this case, the tunability of the metamaterial is achieved by incorporating silicon semiconductor islands on 2 out of the 3 gaps of the SRRs, as shown in Figure 10. Other than that the experimental approach is the same as previously only that this time the photoexcitation will affect only the 2 gaps. At high laser fluence levels, the photoexcited silicon islands will completely short-circuit the 2 gaps, leaving the metamaterial only with one and thus a completely different resonance mode.

This is indeed depicted in the experimental results shown in Figure 11(a), where the THz transmission spectrum is plotted as a function of the laser pump fluence. As the pump energy flux increases, the observed resonance at 0.76 THz starts to weaken while it

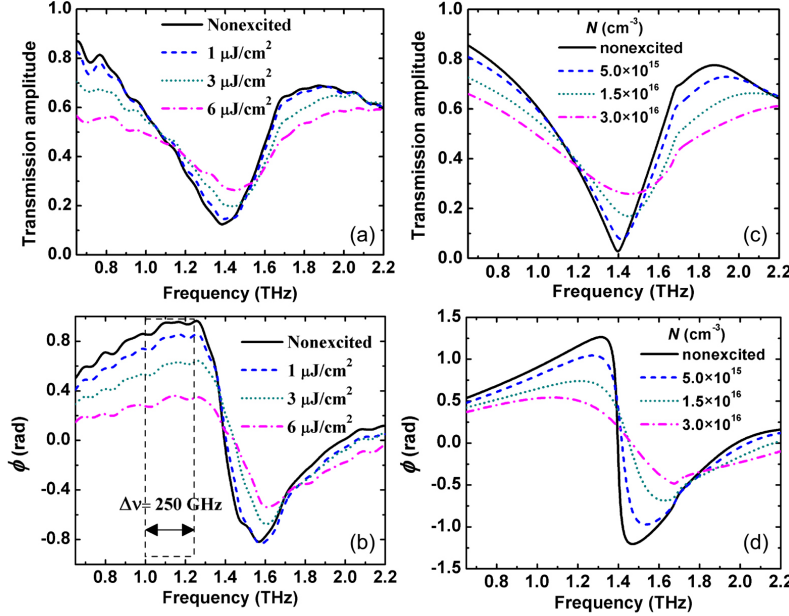


FIG. 9: (a) Experimental results of THz transmission spectra and (b) phase tenability as function of the energy flux of the laser pump beam. (c) and (d) present the respective theoretical results as extracted for different levels of carriers density within the GaAs substrate.

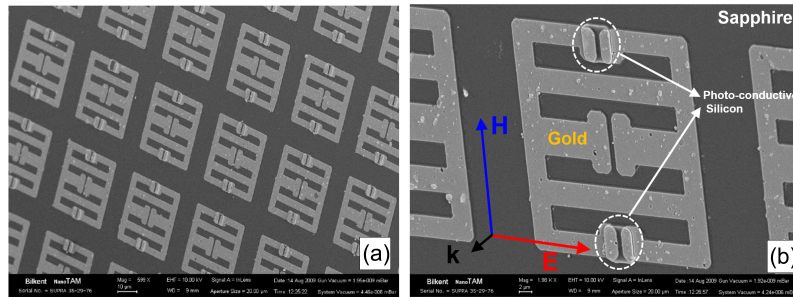


FIG. 10: Optical microscopy images of the hybrid metamaterial. (a) Large area of the metamaterial, (b) close view of the unit cell where the inclusions of photoconductive silicon within the gaps can be seen.

is significantly shifted to higher frequencies resulting to a new resonance peak located at 0.96 THz (red line). This corresponds to a fairly broadband blue-shift of 26% in the resonance frequency. As a comparison and for interpreting the experimental demonstrations, numerical simulations have been performed using the commercial software CST Microwave Studio which are overall in quite good agreement with the experimental observations (Figure 11(b)). The experimentally observed and theoretically calculated, broadband blueshift tunability of the resonance response of the hybrid THz metamaterial demonstrates the po-

tential of achieving ultrafast THz switches, opening thus, a new path to exploring more designs targeting greater flexibility for practical applications in the range of frequency-agile metamaterials [31].

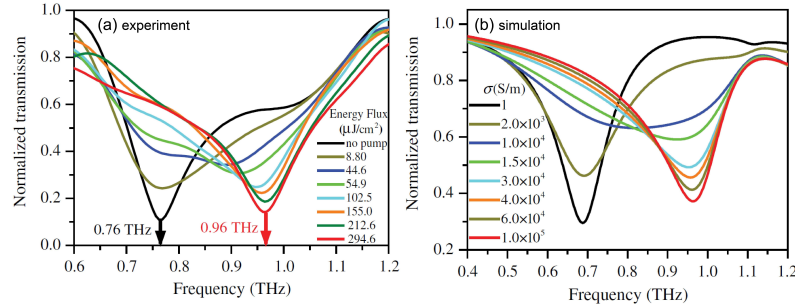


FIG. 11: (a) Normalized transmission of the THz beam pulse, as measured experimentally, for different energy flux of the IR laser beam irradiating the metamaterial. A clear switch-effect of the resonance frequency appears at high photo-excitation levels. (b) Results of simulations for different values of silicon's conductivity as calculated for the respective experimental values of the energy flux of pump beam.

Both of the aforementioned metamaterial designs have been fabricated following lithographic approaches where the desired THz response is achieved by designing properly metallic structures. An alternative way to have fascinating metamaterial properties and possibilities in the THz range, like negative refractive index [34], and/or manipulate the dispersion of THz waves in unique ways [35], is to use properly structured polaritonic materials.

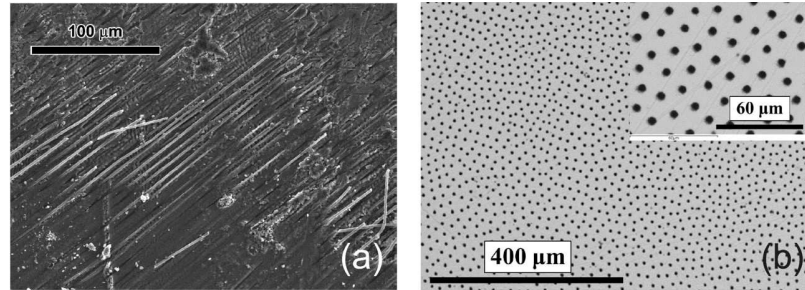


FIG. 12: (a) Scanning electron microscopy (SEM) image of polished longitudinal section of the eutectic LiF/KCl. In bright phase are shown the long continuous LiF rods lattice embedded in KCl matrix (dark phase). (b) SEM image of the transverse cross-section of LiF/KCl eutectic sample grown at 2 mm/h pulling rate.

The third metamaterial system presented in this review paper is fabricated employing the eutectic directional solidification technique [36] which has been proven extremely suitable for achieving polaritonic metamaterial structures. Following this self-organization approach, a 2D periodic polaritonic system of long and continuous LiF rods embedded in

a KCl host has been fabricated (Figure 12). According to recent theoretical studies, an enhancement of E/M wave transmission through an epsilon-near-zero (ENZ) material is expected if dielectric cylinders are embedded in it [37], a transmission which is associated with subwavelength guiding effects. In the case of the eutectic polaritonic LiF/KCl system where, the KCl host shows an epsilon-near-zero (ENZ) response around 6 THz, ($\epsilon_{KCl} \sim 0$), while the LiF has a dielectric-like response [38], with $\epsilon_{LiF} = 15.5$ at ~ 6 THz, similar phenomena are expected.

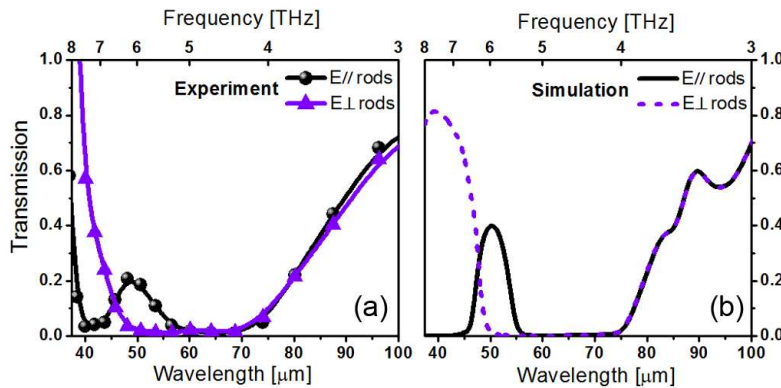


FIG. 13: (a) THz transmission spectra, through a 60 m thick, LiF/KCl system, as recorded for a polarization of the THz electric field parallel (circles) and perpendicular (triangles) to the LiF rods lattice, (b) THz transmission through the sample as simulated using the CST Microwave studio.

In Figure 13(a) are presented the THz transmission spectra through a longitudinally sliced LiF/KCl eutectic as measured for two different orientations of the LiF rods to the incident THz electric field, within the frequency range between 3.0 and 8.0 THz. As one can clearly see, in the case of perpendicular polarization the eutectic system exhibits zero transmission between 4.3 THz to 6.2 THz. On the other hand, for parallel polarization, a broad transmission peak appears centered around 6 THz, at the frequency where the KCl host of the eutectic exhibits near-zero permittivity. Similar response is predicted from theoretical calculations (Figure 13(b)) indicating that the experimentally observed transmission peak at 6 THz is an enhanced transmission associated with Mie-resonances in the LiF rods and the ENZ response of the KCl host, at this frequency. An additional feature characterizing this resonant response is associated with an electric field which is strongly confined along the direction of the incident wave. As theoretically calculated and presented in Figure 14, the electric field amplitude of a plane wave of 6 THz frequency as propagating through a microstructured system with features similar to the experimentally studied one, is sub-wavelength waveguided within the microstructures of the ENZ eutectic material. These theoretical predictions along with the experimental observations show a new way for realizing simple sub-wavelength waveguides in the THz regime. More details on this work can be found in [33].

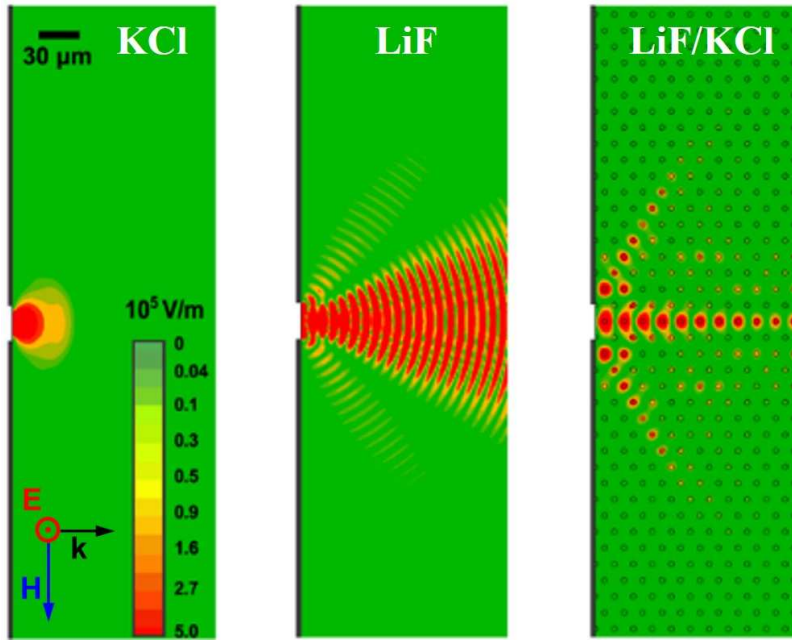


FIG. 14: The electric field amplitude distribution of a plane wave of 6 THz frequency, propagating in a KCl medium (left), LiF (middle) and in a matrix of KCl matrix doped with LiF rods (right), passing through a 15 μm slit.

IV. CONCLUSIONS

In this review, we have presented in details a source yielding ultrashort THz pulses with high peak intensity and broadband frequency spectrum. We have shown ways to tune the emitted THz pulses in terms of duration, strength and polarization by appropriately tailoring the filamentation process, the uniformity and length of the plasma string. One of the most interesting possibilities offered by this tunability is the generation of fully circularly polarized THz light, which will be of great interest in studies like circular dichroism or chirality. Finally, we have shown additional ways of controlling the THz fields using either dynamically controlled metamaterials or cleverly fabricated microstructures based on self-organization which open the way for future large-scale production of THz devices.

Acknowledgements

The authors acknowledge their colleagues that have contributed in parts of this work, J. M. Manceau, M. Kafesaki, C. M. Soukoulis and E. Ozbay and R. I. Merino for the fabrication of the hybrid metamaterials and the eutectic metamaterials respectively. This work was supported in part by the EU Marie Curie Excellence Grant “MULTIRAD” MEXT-CT-2006-042683, the FP7 programs LaserLab-Europe (grant no 284464), CHARISMA (grant

no 228330), ENSEMBLE (grant no 213669), NIMNIL (grant no 228637) and Aristea “FTERA” (grant no 2570) co-financed by the European Union and Greek National Funds.

References

- [1] J. L. Skinner, *Science* **328**, 985 (2010).
- [2] K. Meister *et al.*, *PNAS* **110**, 1617 (2013).
- [3] V. T. Lyubov *et al.*, *Scientific Reports* **3**, (2013).
- [4] N. K. Grady *et al.*, *Science* **340**, 1304 (2013).
- [5] P. U. Jepsen, D. G. Cooke and M. Koch, *Laser Photonics Rev.* **5**, 124 (2011).
- [6] G. Gallot and D. Grischkowsky, *J. Opt. Soc. Am. B* **16**, 1204 (1999).
- [7] M. van Exter, C. Fattinger and D. Grischkowsky, *Appl. Phys. Lett.* **55**, 337 (1989).
- [8] J. A. Fülöp *et al.*, *Opt. Lett.* **37**, 557 (2012).
- [9] E. Matsubara, M. Nagai and M. Ashida, *Appl. Phys. Lett.* **101**, 011105 (2012).
- [10] K. Y. Kim, A. J. Taylor, J. H. Glownia and RodriguezG, *Nat Photon* **2**, 605 (2008).
- [11] T. I. Oh *et al.*, *New J. Phys.* **15**, 075002 (2013).
- [12] I. Z. Nikolay and S. K. Yuri, *Nature Materials* **11**, 917 (2012).
- [13] Q. Wu and X. C. Zhang, *Appl. Phys. Lett.* **68**, 1604 (1996).
- [14] M. v. Exter, C. Fattinger and D. Grischkowsky, *Opt. Lett.* **14**, 1128 (1989).
- [15] I. C. Ho, X. Guo and X. C. Zhang, *Opt. Express* **18**, 2872 (2010).
- [16] J. M. Manceau, P. A. Loukakos and S. Tzortzakis, *Appl. Phys. Lett.* **97**, 251904 (2010).
- [17] L. Mengkun *et al.*, *Nature* **487**, 345 (2012).
- [18] M. Chen, A. Pukhov, X.-Y. Peng and O. Willi, *Physical Review E* **78**, 046406 (2008).
- [19] H. Wen and A. M. Lindenberg, *Phys. Rev. Lett.* **103**, 023902 (2009).
- [20] J.-M. Manceau, M. Massaouti and S. Tzortzakis, *Opt. Express* **18**, 18894 (2010).
- [21] Y. S. You, T. I. Oh and K.-Y. Kim, *Opt. Lett.* **38**, 1034 (2013).
- [22] Y. Chen *et al.*, *Opt. Lett.* **33**, 2731 (2008).
- [23] A. Couairon, H. S. Chakraborty and M. B. Gaarde, *Physical Review A* **77**, 053814 (2008).
- [24] J. M. Manceau *et al.*, *Opt. Lett.* **34**, 2165 (2009).
- [25] J. M. Manceau, M. Massaouti and S. Tzortzakis, *Opt. Lett.* **35**, 2424 (2010).
- [26] T. J. Yen *et al.*, *Science* **303**, 1494 (2004).
- [27] H.-T. Chen *et al.*, *Nat Photon* **3**, 148 (2009).
- [28] K. Iwaszcuk *et al.*, *Opt. Express* **20**, 635 (2012).
- [29] N. I. Landy, S. Sajuyigbe, J. J. Mock, D. R. Smith and W. J. Padilla, *Phys. Rev. Lett.* **100**, 207402 (2008).
- [30] H. T. Chen *et al.*, *Nat. Photon.* **2**, 295 (2008).
- [31] N.-H. Shen *et al.*, *Phys. Rev. Lett.* **106**, 037403 (2011).
- [32] J. M. Manceau, N. H. Shen, M. Kafesaki, C. M. Soukoulis and S. Tzortzakis, *Appl. Phys. Lett.* **96**, 021111 (2010).
- [33] M. Massaouti *et al.*, *Opt. Lett.* **38**, 1140 (2013).
- [34] J. A. Schuller, R. Zia, T. Taubner and M. L. Brongersma, *Phys. Rev. Lett.* **99**, 107401 (2007).
- [35] A. A. Basharin, M. Kafesaki, E. N. Economou and C. M. Soukoulis, *Opt. Express* **20**, 12752 (2012).
- [36] J. Llorca and V. M. Orera, *Prog. Mater Sci.* **51**, 711 (2006).
- [37] K. C. Huang, P. Bienstman, J. D. Joannopoulos, K. A. Nelson and S. Fan, *Physical Review B* **68**, 075209 (2003).
- [38] A. Reyes-Coronado, *et al.*, *Opt. Express* **20**, 14663 (2012).